



HAL
open science

Probing the Higgs sector of $Y = 0$ Higgs triplet model at LHC

M. Chabab, M. C Peyranère, L. Rahili

► **To cite this version:**

M. Chabab, M. C Peyranère, L. Rahili. Probing the Higgs sector of $Y = 0$ Higgs triplet model at LHC. European Physical Journal C: Particles and Fields, 2018, 78 (10), 10.1140/epjc/s10052-018-6339-2 . hal-01981705

HAL Id: hal-01981705

<https://hal.science/hal-01981705>

Submitted on 15 Jan 2019

HAL is a multi-disciplinary open access archive for the deposit and dissemination of scientific research documents, whether they are published or not. The documents may come from teaching and research institutions in France or abroad, or from public or private research centers.

L'archive ouverte pluridisciplinaire **HAL**, est destinée au dépôt et à la diffusion de documents scientifiques de niveau recherche, publiés ou non, émanant des établissements d'enseignement et de recherche français ou étrangers, des laboratoires publics ou privés.

Probing the Higgs sector of $Y = 0$ Higgs Triplet Model at LHC

M. Chabab ^{a*}, M. C. Peyranère ^{b†}, L. Rahili ^{a,c‡}

^a *LPHEA, Faculty of Science Semlalia, Cadi Ayyad University, P.O.B. 2390 Marrakech, Morocco*

^b *LUPM, Montpellier University, F-34095 Montpellier, France*

^c *EPTHE, Faculty of Sciences, Ibn Zohr University, P.O.B. 8106 Agadir, Morocco*

Abstract

In this paper, we investigate the Higgs Triplet Model with hypercharge $Y_\Delta = 0$ (HTM0), an extension of the Standard model, characterized by a more involved scalar spectrum consisting of two CP even Higgs h^0, H^0 and two charged Higgs bosons H^\pm . We first show that the parameter space of HTM0, usually delimited by combined constraints originating from unitarity and BFB as well as experimental limits from LEP and LHC, is severely reduced when the modified Veltman conditions at one loop are also imposed. Then, we perform a rigorous analysis of Higgs decays either when h^0 is the SM-like or when the heaviest neutral Higgs H^0 is identified to the observed 125 GeV Higgs boson at LHC. In these scenarios, we perform an extensive parameter scan, in the lower part of the scalar mass spectrum, with a particular focus on the Higgs to Higgs decay modes $H^0 \rightarrow h^0 h^0, H^\pm H^\mp$ leading predominantly to invisible Higgs decays. Finally, we also study the scenario where h^0, H^0 are mass degenerate. We thus find that consistency with LHC signal strengths favours a light charged Higgs with a mass about $176 \sim 178$ GeV.

*mchabab@uca.ac.ma

†michel.capdequi-peyranere@umontpellier.fr

‡rahililarbi@gmail.com

Our analysis shows that the diphoton Higgs decay mode and $H \rightarrow Z\gamma$ are not always positively correlated as claimed in a previous study. Anti-correlation is rather seen in the scenario where h is SM like, while correlation is sensitive to the sign of the potential parameter λ when H is identified to 125 GeV observed Higgs.

1 Introduction

Without a doubt, the neutral scalar boson discovered by ATLAS [1] and CMS [2] at the Large Hadron Collider (LHC) corresponds to the Higgs boson. All data collected at 7 and 8 TeV support the existence of Higgs signal with a mass around 125 GeV with Standard Model (SM) like properties. Moreover, the deviation in $\gamma\gamma$ channel for the gluon and vector boson fusion productions, the Higgs production and decays into WW^* and ZZ^* are all consistent with SM predictions, as can be seen from LHC run II measurements at 13 TeV [3, 4].

Similarly to our previous phenomenological analysis in the type II seesaw model [5–9] we focus in this work on the Higgs Triplet Model with hypercharge $Y_\Delta = 0$, hereafter referred to as HTM0. The main motivation of the HTM0 is related to the mysterious nature of dark matter (DM) and dark energy, which may signal new physics beyond the SM [10–12]. Although a recent analysis of the HTM0 has been done in [13], we revisit this model in light of new data at LHC run II, with the aim to improve the previous analysis of the Higgs decays which suffered from some inconsistencies that produced inappropriate results for the correlation between Higgs to diphoton decay and Higgs to photon and a Z boson. Furthermore, our work will investigate the naturalness problem in HTM0. We will show how the new degrees of freedom in the HTM0 spectrum can soften the quadratic divergencies and how the Veltman conditions are modified accordingly (VC) [14–17]. As a consequence, we will see that the parameter space of our model is severely constrained by the modified Veltman conditions.

This paper is organised as following. In section 2, we briefly review the main features of HTM0, and present the full set of constraints on the parameters of the Higgs potential. Section 3 is devoted to the derivation of the modified VC's in HTM0. The Higgs sector is discussed in greater detail in section 4 where either h^0 or H^0 are identified to the SM-like Higgs, and at last we focus on the scenario of their mass degeneracy where both Higgses mimic the observed ~ 125 GeV. A full set of constraints were taken into account in the various analyses, including

theoretical (BFB, unitarity) as well as the experimental ones, and scrutinised via HiggsBounds v4.2.1 [18] which we use to check agreement with all 2σ exclusion limits from LEP, Tevatron and LHC Higgs searches. Our conclusion is drawn in section 5, while some technical details are postponed into appendices.

2 Review of the HTM0 model

2.1 Lagrangian and Higgs masses

The Higgs triplet model with hypercharge $Y_\Delta = 0$ can be implemented in the Standard Model by adding a colourless scalar field Δ transforming as a triplet under the $SU(2)_L$ gauge group with hypercharge $Y_\Delta = 0$. The most general gauge invariant and renormalisable $SU(2)_L \times U(1)_Y$ Lagrangian of the scalar sector is given by,

$$\begin{aligned} \mathcal{L} &= (D_\mu H)^\dagger (D^\mu H) + Tr(D_\mu \Delta)^\dagger (D^\mu \Delta) \\ &- V(H, \Delta) + \mathcal{L}_{\text{Yukawa}} \end{aligned} \quad (2.1)$$

where the covariant derivatives are defined by,

$$D_\mu H = \partial_\mu H + igT^a W_\mu^a H + i\frac{g'}{2} B_\mu H \quad (2.2)$$

$$D_\mu \Delta = \partial_\mu \Delta + ig[T^a W_\mu^a, \Delta]. \quad (2.3)$$

(W_μ^a, g) , and (B_μ, g') are respectively the $SU(2)_L$ and $U(1)_Y$ gauge fields and couplings and $T^a \equiv \sigma^a/2$, where σ^a ($a = 1, 2, 3$) denote the Pauli matrices. The potential $V(H, \Delta)$ can be expressed as [11],

$$\begin{aligned} V(H, \Delta) &= -m_H^2 H^\dagger H + \frac{\lambda}{4} (H^\dagger H)^2 - M_\Delta^2 Tr(\Delta^\dagger \Delta) + \mu H^\dagger \Delta H \\ &+ \lambda_1 (H^\dagger H) Tr(\Delta^\dagger \Delta) + \lambda_2 (Tr \Delta^\dagger \Delta)^2 + \lambda_3 Tr(\Delta^\dagger \Delta)^2 \\ &+ \lambda_4 H^\dagger \Delta^\dagger \Delta H \end{aligned} \quad (2.4)$$

where Tr is the trace over 2×2 matrices. Last, $\mathcal{L}_{\text{Yukawa}}$ contains all the Yukawa sector of the SM plus an extra Yukawa term that leads after spontaneous symmetry breaking to (Majorana) mass terms for the neutrinos, without requiring right-handed neutrino states.

Defining the electric charge as usual, $Q = I_3 + \frac{Y}{2}$ where I denotes the isospin, we write the two Higgs multiplets in components as:

$$\Delta = \frac{1}{2} \begin{pmatrix} \delta^0 & \sqrt{2}\delta^+ \\ \sqrt{2}\delta^- & -\delta^0 \end{pmatrix} \quad \text{and} \quad H = \begin{pmatrix} \phi^+ \\ \phi^0 \end{pmatrix} \quad (2.5)$$

with

$$\phi^0 = \frac{1}{\sqrt{2}}(v_d + h_1 + i z_1) \quad \text{and} \quad \delta^0 = v_t + h_2 \quad (2.6)$$

For later convenience, the vacuum expectation values v_d and v_t are supposed positive values.

Assuming that spontaneous electroweak symmetry breaking (EWSB) is taking place at some electrically neutral point in the field space, and denoting the corresponding VEVs by

$$\langle \Delta \rangle = \frac{1}{2} \begin{pmatrix} v_t & 0 \\ 0 & -v_t \end{pmatrix} \quad \text{and} \quad \langle H \rangle = \begin{pmatrix} 0 \\ v_d/\sqrt{2} \end{pmatrix} \quad (2.7)$$

one finds, after minimisation of the potential Eq.(2.4), the following necessary conditions :

$$M_{\Delta}^2 = \frac{\lambda_a}{2} v_d^2 - \frac{\mu v_d^2}{4v_t} + \lambda_b v_t^2 \quad (2.8)$$

$$m_H^2 = \frac{\lambda}{4} v_d^2 - \frac{\mu v_t}{2} + \frac{\lambda_a}{2} v_t^2 \quad (2.9)$$

where $\lambda_a = \lambda_1 + \frac{\lambda_4}{2}$ and $\lambda_b = \lambda_2 + \frac{\lambda_3}{2}$.

The 7×7 squared mass matrix,

$$\mathcal{M}^2 = \frac{1}{2} \frac{\partial^2 V}{\partial \eta_i^2} \Big|_{\Delta=\langle \Delta \rangle, H=\langle H \rangle} \quad (2.10)$$

can be cast, thanks to Eqs. (2.8, 2.9), into a block diagonal form of three 2×2 matrices, denoted in the following by \mathcal{M}_{\pm}^2 , $\mathcal{M}_{\mathcal{CP}_{even}}^2$, and one odd eigenstate corresponding to the neutral Goldstone boson G^0 . The mass-matrix for singly charged field given by,

$$\mathcal{M}_{\pm}^2 = \mu \begin{pmatrix} v_t & v_d/2 \\ v_d/2 & v_d^2/4v_t \end{pmatrix}$$

is diagonalised by a 2×2 rotation matrix $\mathcal{R}_{\theta_{\pm}}$, where θ_{\pm} is a rotation angle. Among the two eigenvalues of \mathcal{M}_{\pm}^2 , one is equal to zero indentifying the charged Goldstone boson G^{\pm} , while the other one corresponds to the mass of singly charged Higgs bosons H^{\pm} given by,

$$m_{H^{\pm}}^2 = \frac{(v_d^2 + 4v_t^2)}{4v_t} \mu \quad (2.11)$$

The mass-eigenstate H^\pm and G^\pm are rotated from the Lagrangian fields ϕ^\pm, δ^\pm as follows :

$$G^\pm = +\cos\theta_\pm\phi^\pm + \sin\theta_\pm\delta^\pm \quad (2.12)$$

$$H^\pm = -\sin\theta_\pm\phi^\pm + \cos\theta_\pm\delta^\pm \quad (2.13)$$

Diagonalization of \mathcal{M}_\pm^2 leads to the following relations involving the rotation angle θ_\pm :

$$\mu\frac{v_d^2}{4v_t} = \cos^2\theta_\pm M_{H^\pm}^2 \quad (2.14)$$

$$\frac{\mu v_d}{2} = -\frac{\sin 2\theta_\pm}{2} M_{H^\pm}^2 \quad (2.15)$$

$$\mu v_t = \sin^2\theta_\pm M_{H^\pm}^2 \quad (2.16)$$

since the Goldstone boson G^\pm is massless. These three equations have a unique solution for $\sin\theta_\pm$ and $\cos\theta_\pm$ up to a global sign ambiguity. Indeed, Eq. (2.14) implies $\mu > 0$ in order to forbid tachyonic H^\pm state, since our convention uses $v_t > 0$. Hence, from Eq. (2.15), $\sin\theta_\pm$ and $\cos\theta_\pm$ should have different signs; one gets :

$$\cos\theta_\pm = \epsilon\frac{v_d}{\sqrt{v_d^2 + 4v_t^2}}, \quad \sin\theta_\pm = -\epsilon\frac{2v_t}{\sqrt{v_d^2 + 4v_t^2}} \quad (2.17)$$

with a sign freedom $\epsilon = \pm 1$, which leads to negative $\tan\theta_\pm$.

As to the neutral scalar, its mass matrix reads:

$$\mathcal{M}_{\mathcal{CP}_{even}}^2 = \begin{pmatrix} A & B \\ B & C \end{pmatrix} \quad (2.18)$$

where

$$A = \frac{\lambda}{2}v_d^2, \quad B = \frac{v_d[-\mu + 2\lambda_a v_t]}{2\sqrt{2}}, \quad C = \frac{\mu v_d^2 + 8\lambda_b v_t^3}{8v_t} \quad (2.19)$$

This symmetric matrix is also diagonalised by a 2×2 rotation matrix \mathcal{R}_α , where α denotes the rotation angle in the \mathcal{CP}_{even} sector.

After diagonalization of $\mathcal{M}_{\mathcal{CP}_{even}}^2$, one gets two massive even-parity physical states h^0 and H^0 defined by,

$$h^0 = +c_\alpha h_1 + s_\alpha h_2 \quad (2.20)$$

$$H^0 = -s_\alpha h_1 + c_\alpha h_2 \quad (2.21)$$

Their masses are given by the eigenvalues of $\mathcal{M}_{\mathcal{CP}_{even}}^2$:

$$m_{h^0}^2 = \frac{1}{2}[A + C - \sqrt{(A - C)^2 + 4B^2}] \quad (2.22)$$

$$m_{H^0}^2 = \frac{1}{2}[A + C + \sqrt{(A - C)^2 + 4B^2}] \quad (2.23)$$

so that $m_{H^0} > m_{h^0}$. Note that the lighter state h^0 is not necessarily the lightest of the Higgs sector. Furthermore, the only odd eigenstate leads to one massless Goldstone boson G^0 defined by $G^0 = z_1$.

Once we know the above eigenmasses for the \mathcal{CP}_{even} , one can determine the rotation angle α which controls the field content of the physical states. One has :

$$C = s_\alpha^2 m_{h^0}^2 + c_\alpha^2 m_{H^0}^2 \quad (2.24)$$

$$B = \frac{\sin 2\alpha}{2} (m_{h^0}^2 - m_{H^0}^2) \quad (2.25)$$

$$A = c_\alpha^2 m_{h^0}^2 + s_\alpha^2 m_{H^0}^2 \quad (2.26)$$

Both Eq. (2.24) and Eq. (2.26) should be equivalent upon use of $s_\alpha^2 + c_\alpha^2 = 1$ and Eqs. (2.22, 2.23). Furthermore, s_α, c_α also do not have definite signs, depending on the sign of B . The relative sign between s_α and c_α depends on the values of μ as can be seen from Eqs.(2.25, 2.19). While they will have the same sign and $\tan \alpha > 0$ for most of the allowed μ and λ_1, λ_4 ranges, there will be a small but interesting domain of small μ values and $\tan \alpha < 0$.

Finally, from Eqs. (2.24 - 2.26), it is easy to express α in terms of A, B and C (Eqs. (2.19)) via :

$$\begin{aligned} \sin 2\alpha &= \frac{2B}{\sqrt{(A - C)^2 + 4B^2}} \quad \text{and} \\ \cos 2\alpha &= \frac{A - C}{\sqrt{(A - C)^2 + 4B^2}} \end{aligned} \quad (2.27)$$

2.2 Constraints in the HTM0

The full experimental validation of the HTM0 would require not only evidence for the neutral and charged Higgs states but also the experimental values for the various field couplings in the gauge and matter sectors of the model. Crucial tests would then be driven by the predicted correlations among these measurable quantities. For instance, the μ and λ 's parameters can be

easily expressed in terms of the physical Higgs masses and the mixing angle α as well as the VEV's v_d, v_t , using equations (2.11), (2.24 - 2.26). One finds

$$\lambda_a = \frac{1}{v_t v_d} \left\{ \sqrt{2} s_\alpha c_\alpha (m_{h^0}^2 - m_{H^0}^2) + \frac{2v_t v_d}{v_d^2 + 4v_t^2} m_{H^\pm}^2 \right\} \quad (2.28)$$

$$\lambda_b = \frac{1}{v_t^2} \left\{ s_\alpha^2 m_{h^0}^2 + c_\alpha^2 m_{H^0}^2 - \frac{v_d^2}{2(v_d^2 + 4v_t^2)} m_{H^\pm}^2 \right\} \quad (2.29)$$

$$\lambda = \frac{2}{v_d^2} \{ c_\alpha^2 m_{h^0}^2 + s_\alpha^2 m_{H^0}^2 \} \quad (2.30)$$

$$\mu = \frac{4v_t}{v_d^2 + 4v_t^2} m_{H^\pm}^2 \quad (2.31)$$

The remaining two Lagrangian parameters m_H^2 and M_Δ^2 are then related to the physical parameters through the EWSB conditions Eqs. (2.8, 2.9).

In the Standard Model the custodial symmetry ensures that the ρ parameter, $\rho \equiv \frac{M_W^2}{M_Z^2 \cos^2 \theta_W}$, is 1 at tree level. In the HTM0, it is clear that δ^0 don't contribute to the Z boson mass, and one obtains the Z and W gauge boson masses readily from Eq. (2.7) and the kinetic terms in Eq.(2.1) as

$$M_Z^2 = \frac{(g^2 + g'^2)v_d^2}{4} = \frac{g^2 v_d^2}{4c_w^2} \quad (2.32)$$

$$M_W^2 = \frac{g^2(v_d^2 + 4v_t^2)}{4} \quad (2.33)$$

Hence the modified form of the ρ parameter is $\rho = \frac{v_d^2 + 4v_t^2}{v_d^2}$.

Since we are interested in the limit $v_t \ll v_d$, we rewrite

$$\rho = 1 + 4 \frac{v_t^2}{v_d^2} = 1 + \delta\rho \quad (2.34)$$

with $\delta\rho = 4 \frac{v_t^2}{v_d^2} > 0$ and $\sqrt{v_d^2 + 4v_t^2} = 246$ GeV.

From a global fit to EWPO one obtains the 1σ result [19],

$$\rho_0 = 1.0004_{-0.0004}^{+0.0003} \quad (2.35)$$

Consequently, in what follows, we adopt the bound

$$\left(\frac{2v_t}{v_d} \right)^2 \lesssim 0.0006 \quad \text{or equivalently} \quad v_t \lesssim 3 \text{ GeV} \quad (2.36)$$

The positivity requirement in the singly charged sector, Eq. (2.11), along with our phase convention $v_t > 0$, lead only to positive values of μ . The tachyonless condition in the \mathcal{CP}_{even} sector,

Eqs. (2.22, 2.23), is somewhat more involved and reads :

$$\mu v_d^2 + 4\lambda v_d^2 v_t + 8\lambda_b v_t^3 > 0 \quad (2.37)$$

$$-2\mu^2 v_t + \mu(\lambda v_d^2 + 8\lambda_a v_t^2) + 8(\lambda\lambda_b - \lambda_a^2)v_t^3 > 0 \quad (2.38)$$

The first equation is actually always satisfied thanks to the positivity of μ and the boundedness from below conditions for the potential. The second equation, quadratic in μ , will lead to new constraints on μ in the form of an allowed range

$$\mu_- < \mu < \mu_+ \quad (2.39)$$

The full expressions of μ_{\pm} are given by

$$\mu_{\pm} = \frac{8\lambda_a v_t^2 + \lambda v_d^2 \pm \sqrt{16\lambda\lambda_a v_d^2 v_t^2 + 64\lambda\lambda_b v_t^4 + \lambda^2 v_d^4}}{4v_t} \quad (2.40)$$

Let us discuss their behaviours in the favoured regime $v_t \ll v_d$. In this case one finds a vanishingly small μ_- given by

$$\mu_- = (\lambda_a^2 - \lambda\lambda_b) \frac{8v_t^3}{\lambda v_d^2} + \mathcal{O}(v_t^4) \quad (2.41)$$

and a large μ_+ given by

$$\mu_+ = \frac{\lambda v_d^2}{2v_t} + 4\lambda_a v_t + \mathcal{O}(v_t^2). \quad (2.42)$$

Depending on the signs and magnitudes of the λ 's, lower bound $\mu > 0$ (positivity of Eq. (2.11)) or μ_- will overwhelm the others. Moreover, these no-tachyon bounds will have eventually to be amended by taking into account the existing experimental exclusion limits. This is straightforward for the charged Higgs boson H^{\pm} , thus we define for later reference :

$$\mu_{\min} = \frac{4v_t}{v_d^2 + 4v_t^2} (m_{H^{\pm}}^2)_{\text{exp}} \quad (2.43)$$

where $(m_{H^{\pm}})_{\text{exp}}$ denotes the experimental lower exclusion limit for the charged Higgs boson mass. So μ must be larger than μ_{\min} in order for the mass to satisfy this exclusion limit.

Upon use of Eqs. (2.7, 2.8, 2.9) in Eq.(2.4) one readily finds that the value of the potential at the electroweak minimum, $\langle V \rangle_{\text{EWSB}}$, is given by:

$$\langle V \rangle_{\text{EWSB}} = -\frac{1}{16}(\lambda v_d^4 + 4\lambda_b v_t^4 + 2v_d^2 v_t(2\lambda_a v_t - \mu)) \quad (2.44)$$

Since the potential vanishes at the gauge invariant origin of the field space, $V_{H=0,\Delta=0} = 0$, then spontaneous electroweak symmetry breaking would be energetically disfavoured if $\langle V \rangle_{\text{EWSB}} > 0$. One can thus require as a first approximation the naive bound on μ

$$\mu < \mu_{\text{max}} \equiv \frac{\lambda v_d^2}{2 v_t} + 2 \lambda_a v_t + \mathcal{O}(v_t^2) \quad (2.45)$$

The phenomenological analysis in section 4 is performed in the parameter space scanned by the potential parameters obeying the usual theoretical constraints, namely perturbative unitarity and boundedness from below (BFB). No need to mention that only the scan points that pass all these constraints are considered in our plots.

BFB:

To derive the BFB constraints, we usually consider that the scalar potential, at large field values, is generically dominated by its quartic part :

$$\begin{aligned} V^{(4)}(H, \Delta) &= \lambda(H^\dagger H)^2/4 + \lambda_1(H^\dagger H)Tr(\Delta^\dagger \Delta) \\ &+ \lambda_2(Tr\Delta^\dagger \Delta)^2 + \lambda_3Tr(\Delta^\dagger \Delta)^2 + \lambda_4 H^\dagger \Delta^\dagger \Delta H \end{aligned} \quad (2.46)$$

In this context, it is common to pick up specific field directions or to put some of the couplings to zero. To proceed to the most general case, we adopt the same parameterisation as in [7], where in our model the ξ and ζ parameters are found to be,

$$\xi = \frac{1}{2} \quad \text{and} \quad \zeta = \frac{1}{2} \quad (2.47)$$

The boundedness from below is then equivalent to requiring $V^{(4)} > 0$ for all directions. As a result, the following set of conditions is derived:

$$\lambda \geq 0 \quad \& \quad \lambda_b \geq 0 \quad (2.48)$$

$$\& \quad \lambda_a + \sqrt{\lambda \lambda_b} \geq 0 \quad (2.49)$$

Unitarity [21]:

As for unitarity constraints, they are given by,

$$|\lambda_a| \leq \kappa\pi \quad (2.50)$$

$$|\lambda| \leq 2\kappa\pi \quad (2.51)$$

$$|\lambda_b| \leq \frac{\kappa}{2}\pi \quad (2.52)$$

$$|3\lambda + 10\lambda_b \pm \sqrt{(3\lambda - 10\lambda_b)^2 + 48\lambda_a^2}| \leq 4\kappa\pi \quad (2.53)$$

The details of their derivation are presented in appendix A. Note that the parameter κ is fixed to the value values $\kappa = 8$, since the unitarity formula $|Re(a_0)| \leq \frac{1}{2}$ has been used.

At this stage, by working out analytically these two sets of BFB and unitarity constraints, we can reduce them to a more compact system where the allowed ranges for the λ 's are easily identified. One can obtain a necessary domain for λ, λ_b that does not depend on λ_a , by considering simultaneously Eqs. (2.51 - 2.53) together with Eq. (2.48),

$$0 \leq \lambda \leq \frac{2\kappa}{3}\pi \quad (2.54)$$

$$0 \leq \lambda_b \leq \frac{\kappa}{5}\pi \quad (2.55)$$

$$|\lambda_a| \leq \sqrt{\frac{5}{2}(\lambda - \frac{2}{3}\kappa\pi)(\lambda_b - \frac{\kappa}{5}\pi)} \quad (2.56)$$

We stress here that the above constraints define the largest possible domain for λ, λ_b for any set of allowed values of λ_a . -Note also that, by using Eqs. (2.54-2.55), one can rewrite Eq. (2.53) under the simple form, given by Eq. (2.56), where the dependence on λ_a has been explicitly separated from that on λ, λ_b .

The reduced couplings $g_{\mathcal{H}ff}$ and $g_{\mathcal{H}VV}$ of the Higgs bosons to fermions and W bosons are given in Tab.1, while the trilinear couplings to charged Higgs bosons can be extracted from the Lagrangian as $\mathcal{L} = g_{\mathcal{H}H^\pm H^\mp} \mathcal{H}H^+H^- + g_{ZH^\pm H^\mp} Z(\partial_\mu H^\pm)H^\mp + \dots$. We will use the reduced HTM0 trilinear coupling of \mathcal{H} and Z to H^\pm given by:

$$\begin{aligned} g_{ZH^+H^-} &= \frac{e}{2s_w c_w} (1 - 2c_w^2) s_{\theta_\pm}^2 \\ \tilde{g}_{\mathcal{H}H^+H^-} &= -\frac{s_w}{e} \frac{m_W}{m_{H^+}^2} g_{\mathcal{H}H^+H^-} \end{aligned} \quad (2.57)$$

where e is the electron charge, s_w the sinus of the weak mixing angle, and m_W the mass of the gauge boson W .

\mathcal{H}	$g_{\mathcal{H}ff}$	$g_{\mathcal{H}WW}$	$g_{\mathcal{H}ZZ}$
h^0	c_α/c_{θ_\pm}	$c_{\theta_\pm}c_\alpha - 2s_{\theta_\pm}s_\alpha$	$c_{\theta_\pm}c_\alpha$
H^0	$-s_\alpha/c_{\theta_\pm}$	$-c_{\theta_\pm}s_\alpha - 2s_{\theta_\pm}c_\alpha$	$-c_{\theta_\pm}s_\alpha$

Table 1: The CP-even neutral Higgs couplings to fermions and gauge bosons in the HTM0 *relative* to the SM Higgs couplings. α and θ_\pm are the mixing angles respectively in the CP-even and charged Higgs sectors.

The trilinear coupling $g_{h^0H^+H^-}$ for the light CP-even Higgs boson is given by :

$$g_{h^0H^+H^-} = -\frac{1}{2} \left\{ c_\alpha (-2c_{\theta_\pm}s_{\theta_\pm}\mu + 2\lambda_a c_{\theta_\pm}^2 v_d + \lambda s_{\theta_\pm}^2 v_d) + s_\alpha (4\lambda_b c_{\theta_\pm}^2 v_t + s_{\theta_\pm}^2 (\mu + 2\lambda_a v_t)) \right\} \quad (2.58)$$

The couplings for the heavy Higgs boson are obtained from the previous ones by simple substitutions $g_{H^0H^+H^-} = g_{h^0H^+H^-} [c_\alpha \rightarrow -s_\alpha, s_\alpha \rightarrow c_\alpha]$.

3 Veltman conditions

To derive the Veltman conditions (VC), one just has to collect the quadratic divergencies [22]. There are various ways to do that, and to be on a safer side, we use the dimensional regularisation because this procedure ensures gauge as well as Lorentz invariances. To work out these quadratic divergencies, we follow exactly the procedure of calculations used in our previous work on the Higgs Triplet Model with hypercharge $Y = 2$ [9]. Moreover, it is worth to note that the main difference with [9] is the absence of the CP odd neutral Higgs A^0 and the doubly charged Higgs $H^{\pm\pm}$, from HTM0 spectrum. Also we have calculated the quadratic divergencies of the CP-neutral Higgs H^0 and h^0 tadpoles in a general linear R_ξ gauge respectively, leading to results which are independent of the ξ parameters but depending on the model mixing angles. As noted in [9], it is more convenient to combine these two results to get the tadpoles quadratic divergencies of the real neutral components of the doublet (h_1) and triplet (h_2) which are free of any mixing angles. After their VEV shifts, one finds, for the doublet:

$$T_d = v_d \left(-2Tr(I_n)\Sigma_f \frac{m_f^2}{v_d^2} + 3(\lambda + \lambda_a) + 2\frac{m_W^2}{v_{sm}^2} \left(\frac{1}{c_w^2} + 2 \right) \right)$$

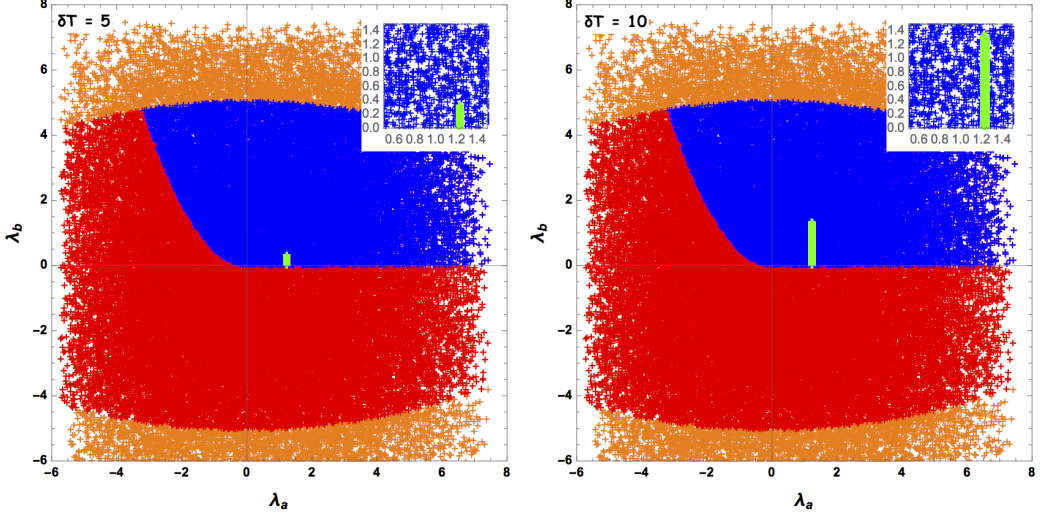


Figure 1: The allowed region in (λ_a, λ_b) for two values of $\delta T = 5, 10$. Color codes are as follows, **Orange** : Excluded by Unitarity constraints. **Red** : Excluded by Unitarity & BFB constraints. **Blue** : Excluded by Unitarity & BFB & VC constraints. The **Green** area represents the ALLOWED region of the parameter space obeying to all theoretical constraints. Our inputs are: $\lambda = 0.52$, $-5 \leq \lambda_1, \lambda_2, \lambda_3, \lambda_4, \lambda_5 \leq 5$, $v_t = 1$ GeV and $2 \leq \mu \leq 5$ (GeV).

where $Tr(I_n)$ is the trace of the n-dimensional identity Dirac matrix, that is $2^{\frac{n}{2}} = 2$ in our case.

For the triplet, one gets :

$$T_t = v_t \left(8 \frac{m_W^2}{v_{sm}^2} + 2\lambda_a + 5\lambda_b \right)$$

In the above expressions, we used the following simplified notations: $c_w = \cos \theta_W$ and $v_{sm} = \sqrt{v_d^2 + v_t^2}$.

Notice that the quadratic divergencies of the Standard Model are easily recovered in T_d when the λ_1 and λ_4 couplings vanish, implying $\lambda_a = 0$.

Now to proceed with the implementation of the two VC's in the parameter space and the subsequent scans, we usually assume that the deviations δT_t and δT_d should not exceed the Higgs mass scale. In our analysis, we will allow them to vary within the reduced conservative range from 0.1 to 10 GeV.

In addition to the theoretical constraints shown in Eqs. 2.49-2.53, namely the unitarity, BFB and $R_{\gamma\gamma}$ from LHC measurements, if the supplementary VC constraints are imposed as well, we see that the allowed region of the parameter space dramatically reduces and its extent

depends on the value given to the deviation δT . This salient feature is illustrated in Fig.1, which exhibits the allowed domain in the (λ_a, λ_b) plan. Our analysis shows that naturalness constraint is stronger than the other theoretical conditions and that deviations δT should be larger than 3 GeV in order to keep a viable model. Moreover, taken those constraints together, one might see that λ_a will be restricted around ~ 1.2 , irrespectively of the value given to the vev v_t . Indeed the same trends described above are reproduced when varying the triplet vev , though the λ_a is somehow freezer out.

Given the above discussed feature, in the next section, our phenomenological analysis will be performed within larger regions of parameter space that omit the VC constraints.

4 Results and Discussions

Since HTM0 spectrum contains two CP even Higgs boson h^0 and H^0 , either h^0 or H^0 can be identified as the observed SM-like boson with mass $\approx 125\text{GeV}$. Therefore, we are facing two choices: $M_h^0 \approx 125$ and $M_h^0 \leq M_H^0$, or $M_H^0 \approx 125$ and $M_h^0 \leq M_H^0$. For the former scenario, the mixing angle limit must verify $\cos \alpha \geq 0.96$, whereas when H^0 mimics the observed boson $\cos \alpha$ tends to a tiny value, so to keep consistency with the experimental data, we imposed $\sin \alpha \geq 0.96$. The third scenario considered in this paper is when both Higgs bosons are mass degenerate, $M_h^0 \approx M_H^0$.

For evaluating the branching ratios we have taken into account the leading perturbative QCD corrections to the two CP-even Higgs decays into hadronic two-body final states. For the Higgs to diphoton and photon+Z gauge boson signal strengths, $R_{\gamma\gamma}$ and $R_{Z\gamma}$, we use the definition adopted in [28],

$$R_{\gamma\gamma(Z\gamma)}(\phi) = \frac{\Gamma_{\phi \rightarrow gg}^{HTM} \times BR_{\phi \rightarrow \gamma\gamma(Z\gamma)}^{HTM}}{\Gamma_{H \rightarrow gg}^{SM} \times BR_{H \rightarrow \gamma\gamma(Z\gamma)}^{SM}} \quad (4.1)$$

The relevant ratios for the other channels $b\bar{b}$, $\tau^+\tau^-$, W^+W^- and ZZ are defined in a similar way. For the constraints and bounds from their corresponding signal strength measurements, we require agreement with the ATLAS and CMS at least at 1σ (see Appendix C for compilation of these signal strengths). Our analyse shows that their ratios remain compatible with respect to its SM values since their \mathcal{H} couplings are almost ≈ 1 .

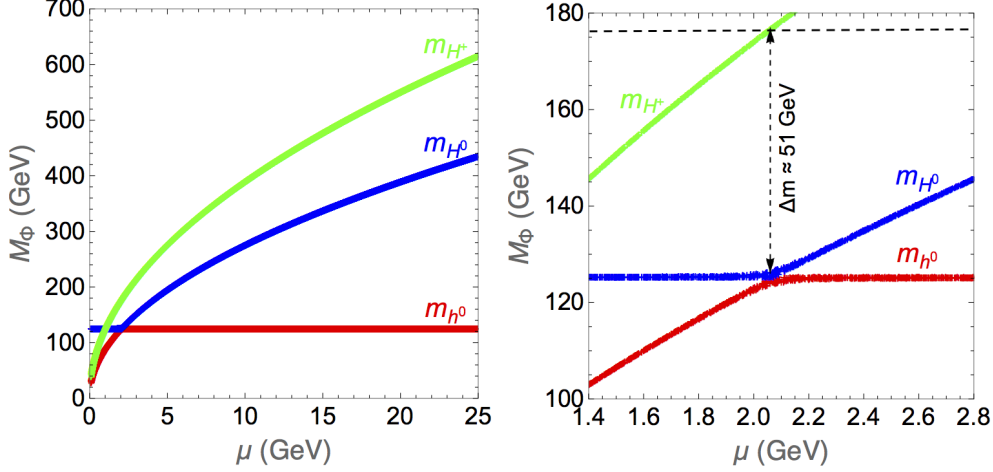


Figure 2: Higgs bosons masses as a function of μ parameter in the HTM0. We take as inputs $\lambda = 0.52$, $-1 \leq \lambda_a \leq 1$, $\lambda_b = 1$, $v_t = 1$ GeV and $0.1 \leq \mu \leq 25$ (GeV).

Also, It should also be noted that for the CP-even Higgs decays to final states with b quarks, the QCD corrections up to three-loops have been included in their partial decay widths [23],

$$\Gamma_{\mathcal{H} \rightarrow q\bar{q}} = \frac{3G_F m_{\mathcal{H}}}{4\sqrt{2}\pi} \bar{m}_q^2(m_{\mathcal{H}}) C_{qq}^{\mathcal{H}} \Delta_{\text{QCD}} \quad (4.2)$$

where

$$\begin{aligned} \Delta_{\text{QCD}} = & \left(1 + 5.67 \frac{\alpha_s(m_{\mathcal{H}})}{\pi} + (35.94 - 1.36N_F) \frac{\alpha_s^2(m_{\mathcal{H}})}{\pi^2} \right. \\ & \left. + (164.14 - 25.77N_F + 0.259N_F^2) \frac{\alpha_s^3(m_{\mathcal{H}})}{\pi^3} \right) \end{aligned} \quad (4.3)$$

For each benchmark scenario, we investigate the allowed parameters space by the 1σ limit of the current Higgs data after run-II in the $gg \rightarrow \mathcal{H} \rightarrow \gamma\gamma$ channel, reported by ATLAS $\mu_{\gamma\gamma} = 0.85^{+0.22}_{-0.20}$ [24–26] and CMS $\mu_{\gamma\gamma} = 1.11^{+0.19}_{-0.18}$ [27], which are consistent with the Standard Model expectation either for ATLAS or for CMS at 1σ . It is worth noting that the errors reported here are smaller than those reported at $7 \oplus 8$ TeV.

4.1 h^0 SM-like

Fig. 3 displays the allowed region in the (v_t, μ) , (μ, m_{H^0}) and (μ, m_{H^\pm}) planes, where h^0 is chosen to be SM-like. It is interesting to note that significant amount of parameter space is allowed once we impose either theoretical or experimental constraints, even for small nonzero value of v_t and μ .

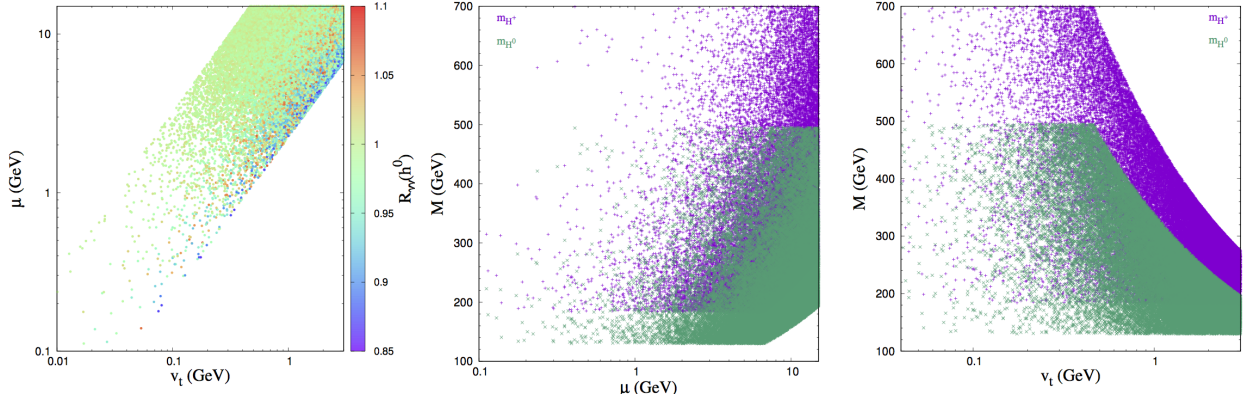


Figure 3: $R_{\gamma\gamma}(h^0)$ variation in the (μ, v_t) plane (left), H^0 and H^\pm Higgs bosons masses as a function of μ (middle) and of v_t (right). Inputs are: $\lambda \approx 0.52$ ($m_{h^0} \approx 125$ GeV), $|\lambda_a| \leq 1.5$, $|\lambda_b| \leq 1$, $10^{-2} \leq \mu \leq 25$ (GeV) and $10^{-2} \leq v_t \leq 3$ (GeV)

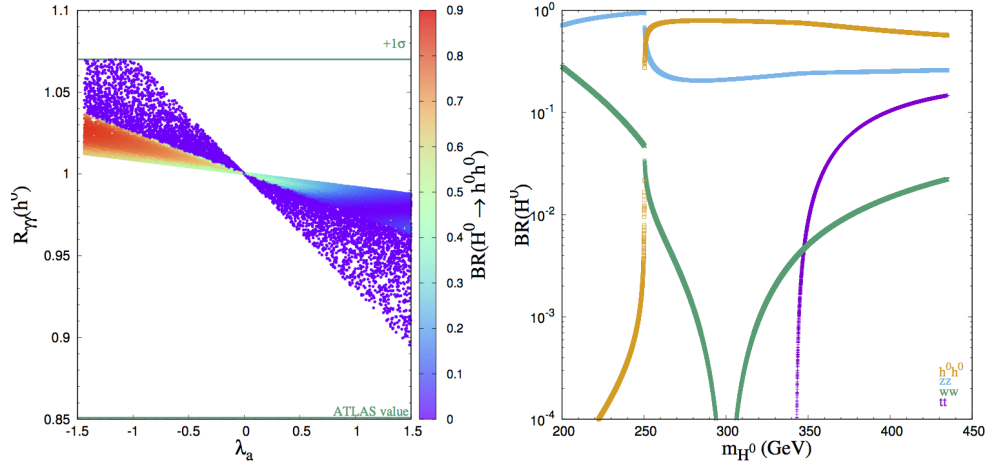


Figure 4: $\text{BR}(H^0 \rightarrow h^0 h^0)$ variation in the $(R_{\gamma\gamma}(h^0), \lambda_a)$ plane taking into account ATLAS result at 1σ , with the following inputs : $\lambda \approx 0.52$, $|\lambda_a| \leq 1.5$, $\lambda_b = 1$, $5 \leq \mu \leq 25$ (GeV) and $v_t = 1$ GeV (left). The $\text{BR}(H^0)$ as a function of m_{H^0} for a benchmark point where $\lambda_a = -1$ (right)

In order to establish in this case the branching ratios of the heaviest CP even neutral Higgs boson, we present in Fig. 4 (right) the decay branching fractions of the heavier Higgs boson H^0 in the HTM0, for a benchmark point where $\lambda_a = -1$. We see that for $200 \text{ GeV} < m_{H^0} < 250 \text{ GeV}$, the dominant decay channels are the $H^0 \rightarrow ZZ$ and W^+W^- decay modes, whereas $h^0 h^0$ is off-shell and consequently its corresponding ratio gets a tiny values of order of 1%, regardless of what λ_a can be. Once $h^0 h^0$ threshold takes place, this channel becomes predominant for

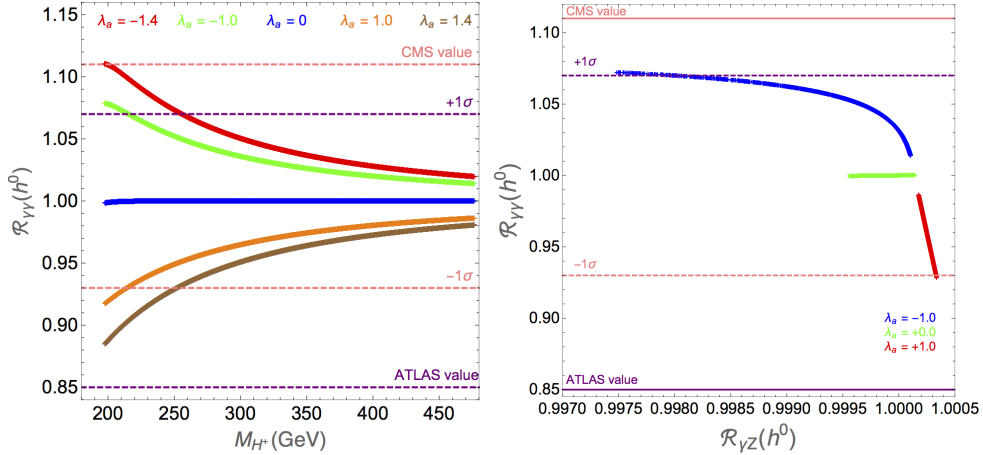


Figure 5: $R_{\gamma\gamma}(h^0)$ as a function of m_{H^\pm} for various values of λ_a (left). Correlation between $R_{\gamma\gamma}(h^0)$ and $R_{\gamma Z}(h^0)$ for various of λ_a (right). We take as inputs : $\lambda \approx 0.52$, $2.5 \leq \mu \leq 15$ (GeV) ($m_{h^0} \approx 125$ GeV), $\lambda_b = 1$ and $v_t = 1$ GeV.

negative λ_a , with the ratio $R_{\gamma\gamma}(h^0)$ almost equal to its standard value, and $250 \leq m_{H^0} < 450$ (GeV). This feature persists even when $t\bar{t}$ threshold is reached at $m_{H^0} > 350$ GeV.

According to Eq. 4.1, we display the deficit of $R_{\gamma\gamma}(h^0)$ in the left panel of Fig. 5 as a function of H^\pm mass for various values of λ_a and with $m_{H^0} \geq 140$ GeV. As it can be seen, a mass about 255 GeV and above is allowed for H^\pm within $+1\sigma$ of ATLAS value for $\lambda_a = -1.4$. Once λ_a increases, this lower bound decreases consistently to reach its lowest value around ~ 197 GeV, given $\lambda_a > -0.5$. This situation is exactly the opposite for CMS, where only the range $200 \leq m_{H^\pm} \leq 250$ (GeV) is excluded for $\lambda_a = 1.4$. Besides, $R_{\gamma\gamma}(h^0)$ tends towards its standard value for $\lambda_a \neq 0$, and to 1 for large m_{H^\pm} whatever the variation of λ_a .

In this scenario, the anti-correlation between $R_{\gamma\gamma}(h^0)$ and $R_{\gamma Z}(h^0)$ is displayed in the left panel of Fig. 5, taking into account the experimental data at 1σ . At first sight, the $R_{\gamma Z}(h^0)$ deviation is almost nul relatively to its standard value, and contrary to what has been claimed in [13], $R_{\gamma\gamma}(h^0)$ and $R_{\gamma Z}(h^0)$ are always anti-correlated, independently of λ_a sign.

4.2 H^0 SM-like invisible decays

This section investigates the possible existence of a scalar state h^0 lighter than H^0 , with $M_{H^0}^0 \approx 125$. Such a scenario has attracted attention within a plethora of theoretical frameworks dealing with new physics beyond standard model, particularly those considering enlargement of the

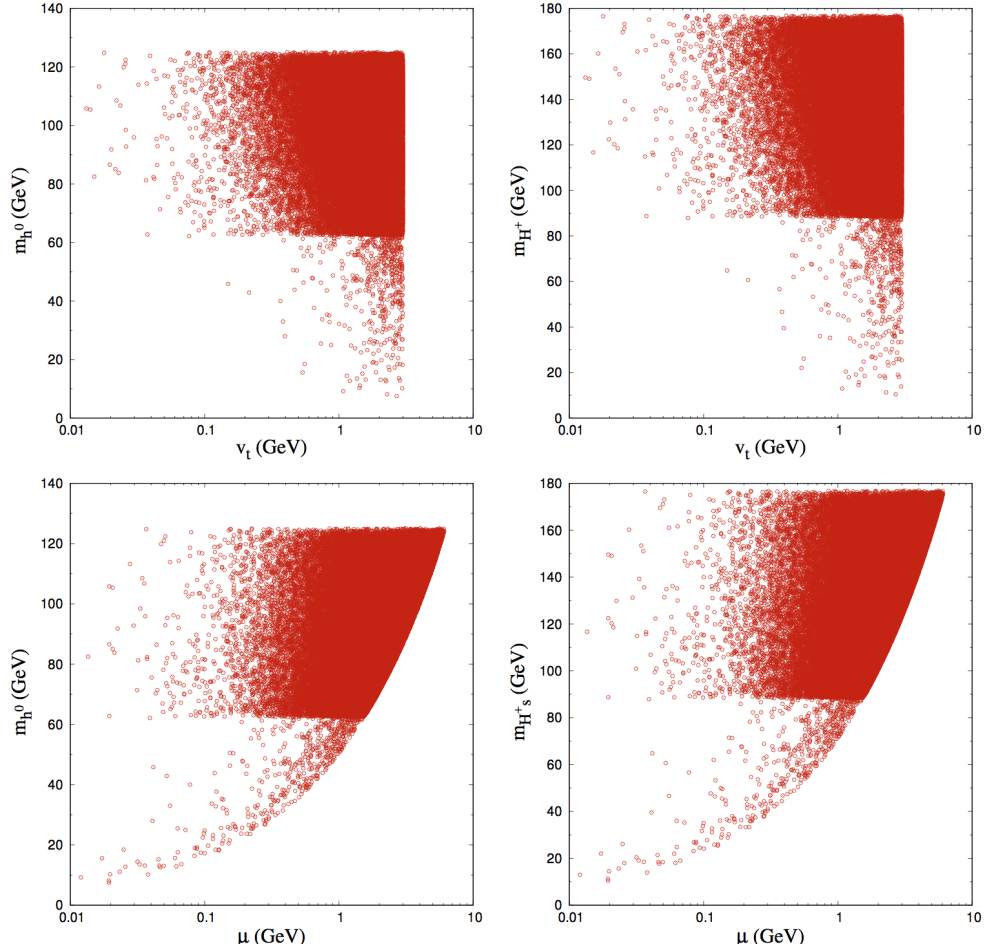


Figure 6: m_{h^0} (left) and m_{H^\pm} (right) dependences on v_t (upper panel) and μ (lower panel). Input parameters are: $\lambda \approx 0.52$ ($m_{H^0} \approx 125$ GeV), $|\lambda_a| \leq 1.5$, $0 \leq \lambda_b \leq 1$, $10^{-2} \leq \mu \leq 10$ (GeV) and $10^{-2} \leq v_t \leq 3$ (GeV)

Higgs sector of the SM via doublet or triplet fields [29, 30]. However, to our knowledge, it has not been addressed yet in the HTM0.

The figure 6 displays the dependence of light and charge Higgs bosons masses on μ and v_t parameters when the heavier CP-even state H^0 is identified to the SM-like Higgs boson. At first glance, the default values of these parameters for a given region where $m_{h^0} \leq \frac{m_{H^0}}{2}$ should not be of the same order of magnitude, indeed, to fulfil such situation, we request v_t to be equal or slightly higher than 1 GeV for a given μ below 1 GeV. As a results, the parameter space is quite restricted offering many new interesting features. Indeed, the charged Higgs is very light with an upper bound on its mass about 180 GeV, as can be seen from Eq. (2.11).

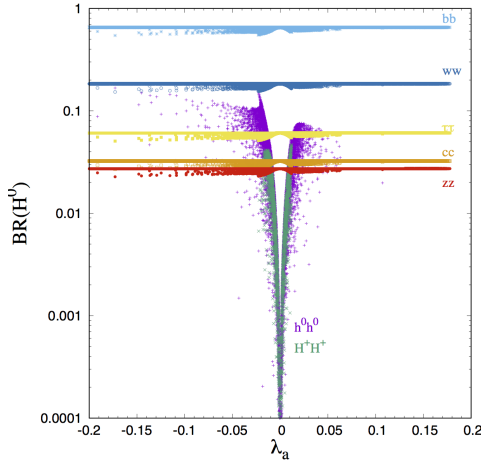


Figure 7: Branching ratio of $H^0 \rightarrow b\bar{b}, c\bar{c}, \tau^+\tau^-, W^+W^-, ZZ, h^0h^0$ and $H^\pm H^\mp$ as a function of λ_a . Our inputs are $\lambda \approx 0.52, \lambda_b = 1, v_t = 1$ GeV and $0.1 \leq \mu \leq 0.52$ (GeV) ($m_{H^0} \approx 125$ GeV).

Moreover, for such small values of μ , the lightest CP-even state h^0 is mostly dominated by a triplet component and is typically light as can be deduced from Eqs. (2.22- 2.26). Thus, in this scenario the LEP constraints apply to h^0 Higgs. At LEP colliders, the Higgs was searched for essentially in the channel $e^+e^- \rightarrow h^0 Z \rightarrow b\bar{b}Z$ in association with Z boson. From the combined data collected by the LEP experiments, a lower limit on the Higgs mass has been established, $m_h > 114.4$ GeV, as well as a set of upper bounds on the Higgs coupling to Z boson [31, 32]. Hence from these LEP results, one can figure out which region of the parameter space which would be allowed (or excluded). In HTM0 model, the coupling of the lightest Higgs to Z boson coupling $h^0 ZZ$, which is proportional to $c_\alpha = \cos\alpha \approx 0$, is heavily suppressed with respect to that of the SM [29]. Hence, the hZ cross section is drastically reduced and the h^0 Higgs may have a mass below the 114.4 limit, while still being in agreement with the LEP constraints.

It is worth to notice that, according to Eq. (2.30), the mass of the heavier CP-even state H^0 matches the observed value $m_{H^0} \approx 125$ GeV, if the coupling λ is approximately set to the value $\lambda \approx 0.52$. Such scenario offers a particularly rich phenomenology. Our analysis will focus on two interesting Higgs to Higgs decays, namely: $H^0 \rightarrow h^0 h^{0(*)}, H^\pm H^{\pm(*)}$. These invisible Higgs decay channels might become kinematically favoured with significant branching ratios for certain regions of the HTM0 parameter space. Indeed, again as $|s_\alpha| \approx 1, c_\alpha \approx 0$ in these

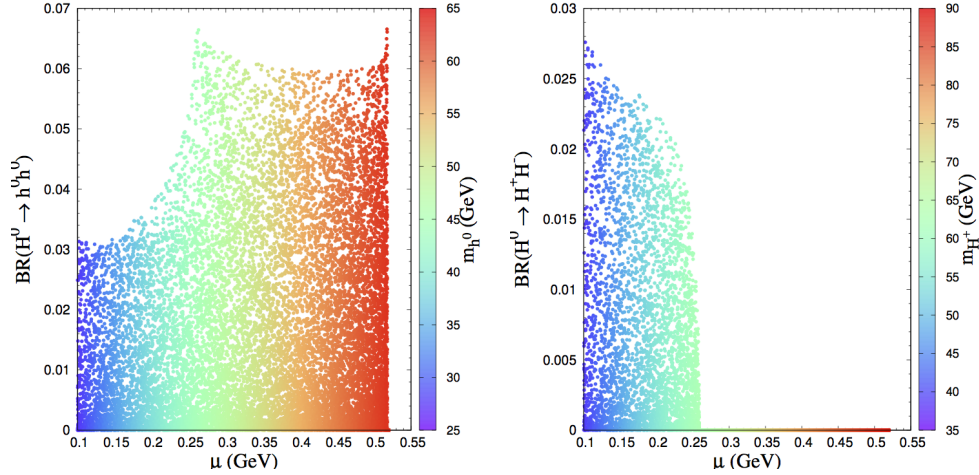


Figure 8: The branching ratios for $H^0 \rightarrow h^0 h^0$ (left) and $H^0 \rightarrow H^\pm H^\mp$ (right) as a function of μ . The Higgs masses, m_{h^0} and m_{H^\pm} , are considered in the ranges represented by the color codes. Our inputs are : $\lambda \approx 0.52$, $10^{-2} \leq \mu \leq 0.55$ (GeV), $m_{H^0} \approx 125$ GeV, $|\lambda_a| \leq 1.5$, $\lambda_b = 1$, and $v_t = 1$ (GeV)

regions, the $h^0 h^0 H^0$ and $H^\pm H^\pm H^0$ couplings reduce to,

$$g_{h^0 h^0 H^0} = g_{H^\pm H^\pm H^0} \simeq \lambda_a v_d + \mathcal{O}(v_t) \quad (4.4)$$

Then, we plot in Fig. 7 the branching ratios of the H^0 decays into $b\bar{b}$, $c\bar{c}$, $W^+W^- ZZ$, and into the invisible decay modes $h^0 h^0$ and $H^\pm H^\mp$. We clearly see that the branching ratios into $h^0 h^0$ and $H^\pm H^\mp$ become dominant for non-vanishing values of $|\lambda_a|$, as can be seen from Eq. (4.4) where the corresponding couplings get substantially large values. However, once λ_a approaches zero, these decay channels fade away.

By the following, we fix $v_t = 1$ GeV and $\lambda_b = 1$, we present in Fig. 8 the branching ratios for $H^0 \rightarrow h^0 h^0$ and $H^0 \rightarrow H^\pm H^\mp$. From the left panel, we can see that decay into $h^0 h^0$ gets sizeable values for values of the μ parameter larger than 0.15 GeV ($m_{h^0} \approx 35$ GeV), reaching up to 7% when m_{h^0} is around 45 ~ 50 GeV. When μ becomes larger than 0.26 GeV ($m_{h^0} \approx 45$ GeV), this ratio decreases slightly but still remains relatively important, and never falls below 6%. Furthermore, for $m_{h^0} \approx 60 \sim 65$ GeV, it raises to reach 7% again.

The situation is quite different for the $\text{BR}(H^0 \rightarrow H^\pm H^\pm)$ as illustrated in the right panel of Fig. 8. This ratio tends to its maximal value, $\approx 2.7\%$, for very tiny μ about ≈ 0.1 GeV, corresponding to small values of $m_{H^\pm} \approx 39$ GeV, and decreases inversely when μ increases up

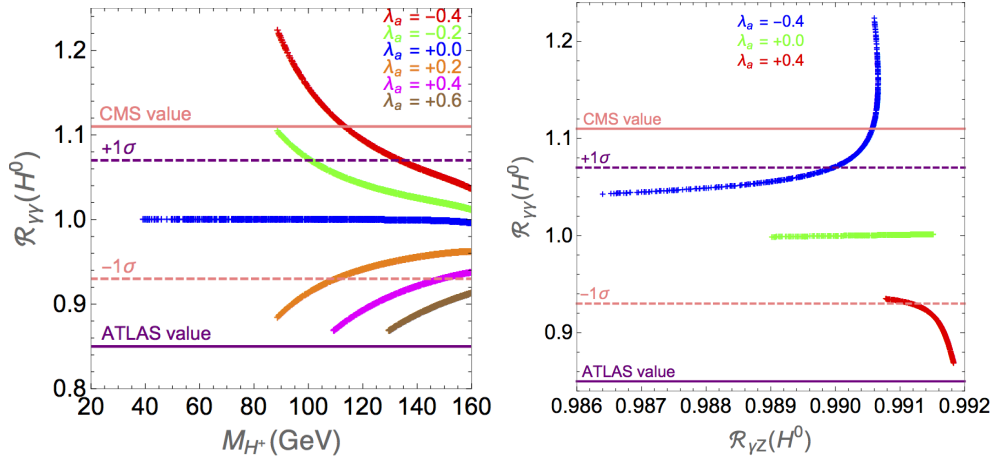


Figure 9: (Left) : $R_{\gamma\gamma}(H^0)$ as a function of m_{H^\pm} for various values of λ_a . (Right) : correlation between $R_{\gamma\gamma}(H^0)$ and $R_{\gamma Z}(H^0)$ for various of λ_a . Our inputs are : $\lambda \approx 0.52$, $0.5 \leq \mu \leq 1.6$ (GeV) ($m_{H^0} \approx 125$ GeV), $\lambda_b = 1$ and $v_t = 1$ GeV.

to the value $\mu \approx 0.26$ GeV. In contrast to the decay into $h^0 h^0$, beyond this value, the branching ratio is almost vanishing.

From the left side of Fig. 9, the ratio $R_{\gamma\gamma}(H^0)$ reaches its SM-like value for $\lambda_a \approx 0$ and for the charged Higgs mass in the range $40 \sim 160$ GeV, while an excess up to 20% can be achieved for negative values of λ_a . If ATLAS/CMS exclusions data at 1σ , is taken into account, then this excess is largely reduced to less than 10%. As a byproduct, this analysis sets up a lower limit on the m_{H^\pm} of order ~ 115 GeV (for $\lambda_a = -0.2$). In addition, $R_{\gamma\gamma}(H^0)$ remains below its SM value when $\lambda_a > 0$, even for m_{H^\pm} above this lower value. At last, we study correlation of $R_{\gamma\gamma}(H^0)$ with $R_{\gamma Z}(H^0)$ in this scenario. Unlike the h^0 SM-like case, one can see from the right panel of Fig. 9 that these observables are correlated for $\lambda_a < 0$ or anti-correlated for $\lambda_a > 0$ with a predicted charged Higgs mass in the range $[130 \sim 160]$ or $[110 \sim 160]$ GeV respectively.

4.3 Degenerate case : $m_{H^0} \approx m_{h^0} \approx 125$ GeV

In this subsection, we consider the CP-even neutral Higgs bosons h^0 and H^0 with nearly degenerate mass. This scenario has recently attracted attention and been taken seriously in many SM extensions [8, 33–35]. Here we would like to ask to what extent this survives in HTM0 in light of LHC data at 13 TeV. In other words, we probe the region of the parameter space where the twin Higgs decays into diphoton Higgs with branching ratio (or signal strength $R_{\gamma\gamma}$)

consistent with ATLAS and CMS data. A first analysis has been performed in [13]. This analysis used an intriguing and unjustified hypothesis considering the charged Higgs mass equals to the neutral ones. In this model, this possibility is excluded by theoretical constraint as we will show shortly. But first, we will demonstrate that the parameter space is restricted further by an additional constraint, induced by the Higgs mass degeneracy, and leading to a severe control of the potential parameters.

The two eigenvalues m_{\pm} (with $m_- = m_{h^0}^2 < m_+ = m_{H^0}^2$), representing the squared masses of h^0 and H^0 , are :

$$m_{\pm} = \frac{A + C \pm \sqrt{(A - C)^2 + 4B^2}}{2}. \quad (4.5)$$

Then

$$\begin{aligned} m_+ - m_- &= (m_{H^0} - m_{h^0})(m_{H^0} + m_{h^0}) \\ &\approx (m_{H^0} - m_{h^0})2M_{ex} = 2M_{ex}\Delta M. \end{aligned}$$

where ΔM , the difference of masses between the two neutral Higgs H^0 and h^0 is set to about 1 GeV, corresponding to the detector inability to resolve two nearly Higgs signals, and M_{ex} is the experimental Higgs boson mass ≈ 125 GeV. Taking into account these considerations one gets $\sqrt{(A - C)^2 + 4B^2} \leq 2M_{ex}\Delta M$, that obviously leads to two constraints: $|B| \leq M_{ex}\Delta M$ and $|A - C| \leq 2M_{ex}\Delta M$.

The first constraint reads as:

$$|2\lambda_a v_t - \mu| \leq 2\sqrt{2} \frac{M_{ex}\Delta M}{v_d}, \quad (4.6)$$

while, for small ratio of the two vevs $\frac{v_t}{v_d}$, the second constraint reduces to,

$$|4\lambda v_t - \mu| \leq \frac{8v_t}{v_d} \frac{2M_{ex}\Delta M}{v_d}, \quad (4.7)$$

Since the ratio $\frac{2M_{ex}\Delta M}{v_d}$ is about 1 GeV, these two relations simplify to $|2\lambda_a v_t - \mu| \leq \sqrt{2}$ GeV and $\frac{\mu}{\lambda} \approx 4v_t$, providing strict bounds to the three potential parameters μ , λ and λ_a , hence severely reducing the allowed regions in the parameter space, as it is illustrated in Fig.10. This feature has a dramatic effect on the discrepancy between the neutral and charged Higgs masses as can be seen from Fig.2. In such figure, the Higgs bosons masse behaviours are plotted as a function of the μ parameter; these values satisfy the above resulting relation in

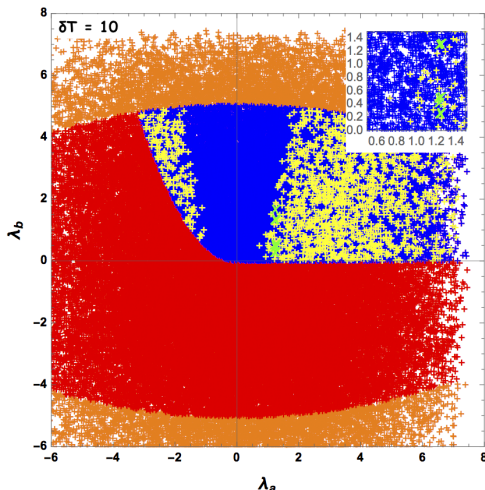


Figure 10: The allowed regions in (λ_a, λ_b) for $\delta T = 10$ in the degenerate case. Color codes are as follows, **Orange** : Excluded by Unitarity constraints. **Red** : Excluded by Unitarity+BFB constraints. **Blue** : Excluded by Unitarity+BFB & $\frac{\mu}{\lambda} \approx 4 v_t$ constraints. **Yellow** : Excluded by Unitarity+BFB & $T_d \approx \delta T \wedge T_t \approx \delta T$ & $\frac{\mu}{\lambda} \approx 4 v_t$ constraints. That shows only the **Green** area obeys ALL constraints. Our inputs are $\lambda = 0.52$, $-5 \leq \lambda_1, \lambda_2, \lambda_3, \lambda_4, \lambda_5 \leq 5$, $10^{-3} \leq v_t \leq 3$ (GeV) and $10^{-3} \leq \mu \leq 5$ (GeV).

the degenerate case. The seemingly constant $m_{h^0}^2$ for $\mu > \mu_c$ and constant $m_{H^0}^2$ for $\mu < \mu_c$ are clearly achieved around the critical value $\mu_c \approx 2.1$ GeV. Contrary to what one might think, if we take the Higgs bosons masses as inputs [13], such a situation matches a splitting between the charged Higgs boson mass and the \mathcal{H} ($= h^0 = H^0$) degenerate state mass in the range of $\Delta m = m_{H^\pm} - m_{\mathcal{H}} \approx 51$ GeV.

Hereafter we define the diphoton signal strength $R_{\gamma\gamma}$ by the following quantity,

$$R_{\gamma\gamma} = R_{\gamma\gamma}(h^0) + R_{\gamma\gamma}(H^0) \quad (4.8)$$

and similarly $R_{\gamma Z}$ is introduced. In this scenario, the charged Higgs boson loops are included with the $g_{\mathcal{H}ww}, g_{\mathcal{H}\bar{f}f}$ couplings given by Table. 1.

Fig. 11 illustrates the HTM0 degenerate case effect on $R_{\gamma\gamma}$. Similarly to the previous scenarios, we fix $\lambda \sim 0.518$ and scan over $\lambda_a, \lambda_b, \mu$ and v_t , with the Higgs masses given by Eqs. 4.5, 4.6 and 4.7. In the left panel, we show the scatter plot for the mixing angle α in the $(R_{\gamma\gamma}, v_t)$ plane. Again we see that small but no zero values below 0.5 are favoured for the triplet vev v_t to achieve the standard limit, corresponding to $\sin \alpha \sim 0.55 - 0.65$. Equally, as

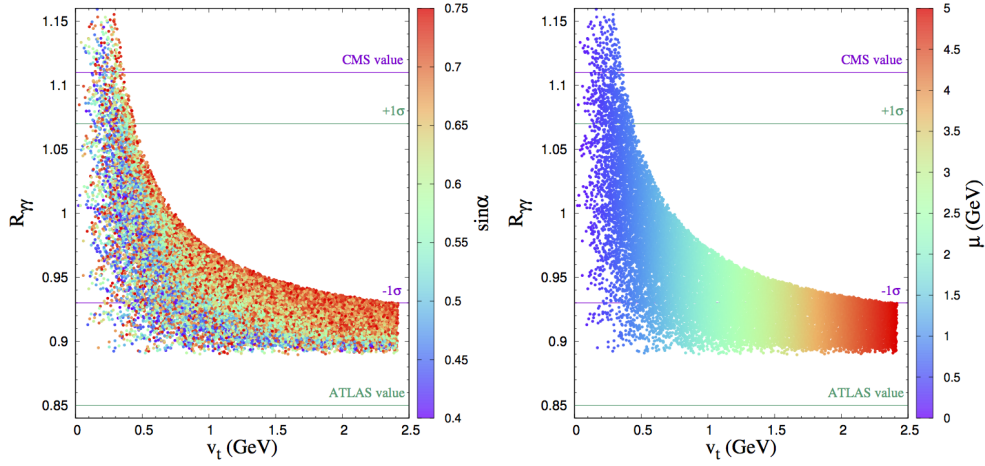


Figure 11: Left: Scatter plot for $\sin \alpha$ in the plan $(R_{\gamma\gamma}, v_t)$ with $10^{-3} \leq \mu \leq 5$ (GeV). Right: $R_{\gamma\gamma}$ as function of v_t , where the palette shows the size of μ .

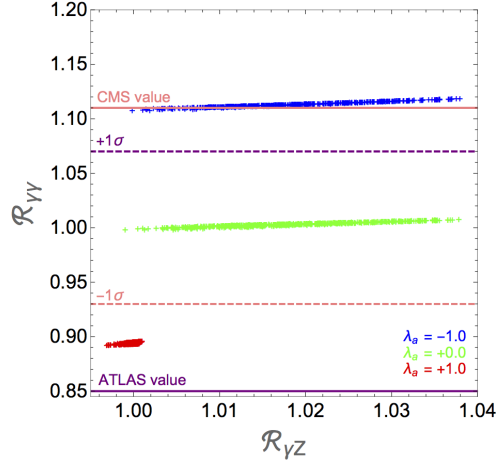


Figure 12: $R_{\gamma\gamma}$ and $R_{\gamma Z}$ correlation in the degenerate case for various λ_a . Inputs are the same as in Fig.11, except for λ_a .

set out from its dependence on v_t in this scenario, the μ parameter takes a tiny values. In the right panel, we show the variation of $R_{\gamma\gamma}$ a function of μ and v_t within 1σ of ATLAS/CMS measurements.

Finally, we display in Fig. 12, we have plotted $R_{\gamma\gamma}$ versus $R_{\gamma Z}$ in mass degenerate scenario for various values of λ_a . From this plot one can see that the correlation is always positive whatever the value of λ_a . We also note that no noticeable enhancement can be achieved, since most part of the parameter space is drastically constrained by a constant charged Higgs mass

at about $m_{H^\pm} \sim 176$ GeV, as shown form Fig. 2, which concurs with the results predicted in [8].

5 Conclusion

In this paper, we have discussed some features of the Higgs triplet model with null hypercharge (HTM0), an extension of the SM with a larger scalar sector. First, we have shown that the parameter space of HTM0 generally constrained by unitarity and boundedness from below, is severely reduced when the modified Veltman conditions are imposed. Then, we have investigated some Higgs decays, including Higgs to Higgs decays, in light of LHC data, either when h^0 is the SM-like Higgs or when the heaviest neutral Higgs H^0 is identified to the 125 observed GeV Higgs. In addition, we have analysed the degenerate scenario and shown that LHC signal strengths favours a light charged Higgs mass about $176 \sim 178$ GeV. Finally, we have pointed out some discrepancies with previous analysis, regarding the correlations between the diphoton Higgs decay mode and $H \rightarrow Z\gamma$ mode.

Acknowledgment

The authors would like to thank G. Moulataka for useful discussions. MC and LR would like to thank LUPM laboratory at Montpellier University for hospitality. This work is supported in part by the Moroccan Ministry of Higher Education and Scientific Research under contract N°PPR/2015/6, and by the GDRI-P2IM: Physique de l'infiniment petit et l'infiniment grand.

Appendix A : Unitarity constraints

By exploring the HTM0 model, we can show that the full set of 2-body scalar scattering processes leads to a 19×19 S-matrix with 5 block of submatrices corresponding to mutually unmixed sets of channels with definite charge and CP states. Hence one gets the following submatrix dimensions, structured in terms of net electric charge in the initial/final states: $S^{(1)}(4 \times 4)$, $S^{(2)}(5 \times 5)$ and $S^{(3)}(1 \times 1)$, corresponding to 0-charge channels, $S^{(4)}(6 \times 6)$ for the 1-charge

channels, and $S^{(5)}(3 \times 3)$ corresponding to the 2-charge channel.

In principle, by using the unitarity equation, one can derive the unitarity constraint on each component of the S-matrix. Thus the usual unitarity bound on partial wave amplitudes would apply to the eigenvalues of the submatrices, encoding indirectly the bounds on all the components $\tilde{T}^{(n)}$ of the T-matrix, defined as $\mathcal{M}_n \equiv i\tilde{T}^{(n)}$, with $n = 1, \dots, 5$.

We present hereafter the resulting submatrices whose entries correspond to the quartic couplings that mediate the $2 \rightarrow 2$ scalar processes. By writing the neutral components in the fields as : $\phi^0 = \frac{1}{\sqrt{2}}(v_d + h_1 + i z_1)$ and $\delta^0 = v_t + h_2$, the first submatrix \mathcal{M}_1 corresponds to scattering whose initial and final states are one of the following: $(\phi^+\delta^-, \delta^+\phi^-, h_2 z_1, h_1 h_2)$. We have to write out the full matrix, one finds,

$$\mathcal{M}_1 = \begin{pmatrix} \lambda_a & 0 & 0 & 0 \\ 0 & \lambda_a & 0 & 0 \\ 0 & 0 & \lambda_a & 0 \\ 0 & 0 & 0 & \lambda_a \end{pmatrix} \quad (5.1)$$

The second submatrix \mathcal{M}_2 corresponds to scattering with one of the following initial and final states: $(\phi^+\phi^-, \delta^+\delta^-, \frac{h_1 h_1}{\sqrt{2}}, \frac{h_2 h_2}{\sqrt{2}}, \frac{z_1 z_1}{\sqrt{2}})$, where the $\sqrt{2}$ accounts for identical particle statistics. From a straightforward calculation, one finds that \mathcal{M}_2 reads as:

$$\mathcal{M}_2 = \begin{pmatrix} \lambda & \lambda_a & \frac{\lambda}{2\sqrt{2}} & \frac{\lambda_a}{\sqrt{2}} & \frac{\lambda}{2\sqrt{2}} \\ \lambda_a & 4\lambda_b & \frac{\lambda_a}{\sqrt{2}} & \sqrt{2}\lambda_b & \frac{\lambda_a}{\sqrt{2}} \\ \frac{\lambda}{2\sqrt{2}} & \frac{\lambda_a}{\sqrt{2}} & \frac{3\lambda}{4} & \frac{\lambda_a}{2} & \frac{\lambda}{4} \\ \frac{\lambda_a}{\sqrt{2}} & \sqrt{2}\lambda_b & \frac{\lambda_a}{2} & 3\lambda_b & \frac{\lambda_a}{2} \\ \frac{\lambda}{2\sqrt{2}} & \frac{\lambda_a}{\sqrt{2}} & \frac{\lambda}{4} & \frac{\lambda_a}{2} & \frac{3\lambda}{4} \end{pmatrix} \quad (5.2)$$

Despite its apparently complicated structure, the seven eigenvalues of \mathcal{M}_2 can be easily determined. At last, for the 0-charge $2 \rightarrow 2$ processus, there is just one state $h_1 z_1$ leading to $\mathcal{M}_3 = \lambda/2$

On the other hand, the 1-charge channels occur for two-by-two body scattering between the charged states $(h_1\phi^+, z_1\phi^+, h_2\phi^+, h_1\delta^+, z_1\delta^+, h_2\delta^+)$. The 6×6 submatrix \mathcal{M}_4 obtained from

the above scattering processes is given by:

$$\mathcal{M}_4 = \begin{pmatrix} \frac{\lambda}{2} & 0 & 0 & 0 & 0 & 0 \\ 0 & \frac{\lambda}{2} & 0 & 0 & 0 & 0 \\ 0 & 0 & \lambda_a & 0 & 0 & 0 \\ 0 & 0 & 0 & \lambda_a & 0 & 0 \\ 0 & 0 & 0 & 0 & \lambda_a & 0 \\ 0 & 0 & 0 & 0 & 0 & 2\lambda_b \end{pmatrix} \quad (5.3)$$

while the fifth submatrix \mathcal{M}_5 corresponds to scattering with initial and final states being one of the following 3 sates: $(\frac{\phi^+\phi^+}{\sqrt{2}}, \frac{\delta^+\delta^+}{\sqrt{2}}, \delta^+\phi^+)$. It reads,

$$\mathcal{M}_5 = \begin{pmatrix} \frac{\lambda}{2} & 0 & 0 \\ 0 & 2\lambda_b & 0 \\ 0 & 0 & \lambda_a \end{pmatrix} \quad (5.4)$$

From the usual expansion in terms of partial-wave amplitudes a_J , we write, following our notations,

$$\mathcal{M}^{(kf)} = i\tilde{T}_{kf} = 16i\pi \sum_{J \geq 0} (2J+1) a_J^{(kf)}(s) P_J(\cos \theta) \quad (5.5)$$

where k and f run over all possible initial and final states of the above 19-state basis and the P_J 's are the Legendre polynomials. Since we only consider the leading high energy contributions for each channel, all the partial waves with $J \neq 0$ vanish, except one:

$$a_0^{(kf)} = -\frac{i}{16\pi} \mathcal{M}^{(kf)} \quad (5.6)$$

The S-matrix unitarity constraint for elastic scattering, $|a_0^{(kk)}| \leq 1$ or alternatively $|Re(a_0^{(kk)})| \leq \frac{1}{2}$, translates through Eq. (5.6) directly to all the eigenvalues of the submatrices we determined above.

Appendix B : Feynman Rules for tadpoles

In this appendix, we list the couplings used to calculate the tadpoles of the two neutral CP-even Higgs h^0 and H^0 as explained in [9].

We note $c_{F_i \bar{F}_i}$ ($C_{F_i \bar{F}_i}$) the couplings to the Higgs h^0 (H^0) where F_i stands for any quantum field of the HTM0: scalar and vectorial bosons, fermions, Goldstone fields G_i and Faddeev-Popov ghost fields η_i . Because the field F_i fixes the propagator, we also list the values t_i (T_i) of the loop due to the propagator of the F_i particle which gain a factor 2 in case of charged fields, and the symmetry factor s_i .

$$\begin{aligned}
c_1 &\equiv c_{h_0 h_0} = -\frac{3i}{2}(\lambda v_d c_\alpha^3 + 2\lambda_a v_d c_\alpha s_\alpha^2 + 4\lambda_b v_t s_\alpha^3 + \\
&\quad (-\mu + 2\lambda_a v_t) c_\alpha^2 s_\alpha), \\
C_1 &\equiv C_{H_0 H_0} = \frac{3i}{2}(\lambda v_d s_\alpha^3 + 2\lambda_a v_d s_\alpha c_\alpha^2 - 4\lambda_b v_t c_\alpha^3 - \\
&\quad (-\mu + 2\lambda_a v_t) s_\alpha^2 c_\alpha), \\
t_1 &= iA_0(m_{h_0}^2), \\
T_1 &= iA_0(m_{H_0}^2), \\
s_1 &= \frac{1}{2},
\end{aligned} \tag{5.7}$$

$$\begin{aligned}
c_2 &\equiv c_{G_0 G_0} = -\frac{i}{2}(-\mu s_\alpha + \lambda v_d c_\alpha + 2\lambda_a s_\alpha v_t), \\
C_2 &\equiv C_{G_0 G_0} = +\frac{i}{2}(\mu c_\alpha + \lambda v_d s_\alpha - 2\lambda_a c_\alpha v_t), \\
t_2 &= T_2 = iA_0(\xi_Z m_Z^2), \\
s_2 &= \frac{1}{2},
\end{aligned} \tag{5.8}$$

$$\begin{aligned}
c_3 &\equiv c_{G_+ G_-} = -\frac{i}{2}(2\mu c_\alpha c_{\theta_\pm} s_{\theta_\pm} + (\mu s_\alpha + \lambda v_d c_\alpha + 2\lambda_a v_t s_\alpha) c_{\theta_\pm}^2 \\
&\quad + 2(\lambda v_d c_\alpha + 2\lambda_b v_t s_\alpha) s_{\theta_\pm}^2), \\
C_3 &\equiv C_{G_+ G_-} = -\frac{i}{2}(-(2\mu c_{\theta_\pm} s_{\theta_\pm} + \lambda v_d c_{\theta_\pm}^2 + 2\lambda_a v_d s_{\theta_\pm}^2) s_\alpha \\
&\quad + (4\lambda_b s_{\theta_\pm}^2 v_t + 2\lambda_a v_t c_{\theta_\pm}^2 + \mu c_{\theta_\pm}^2) c_\alpha), \\
t_3 &= T_3 = 2 \times iA_0(\xi_W m_W^2), \\
s_3 &= \frac{1}{2},
\end{aligned} \tag{5.9}$$

$$\begin{aligned}
c_4 &\equiv c_{H_0 H_0} = -\frac{i}{2}(2\lambda_a c_\alpha^3 v_d + (3\lambda - 4\lambda_a) c_\alpha s_\alpha^2 v_d - (\mu - \\
&\quad 2\lambda_a v_t) s_\alpha^3 + 2c_\alpha^2 s_\alpha (\mu - 2(\lambda_a - 3\lambda_b) v_t)) \\
C_4 &\equiv C_{h_0 h_0} = -\frac{i}{2}(-2\lambda_a s_\alpha^3 v_d - (3\lambda - 4\lambda_a) s_\alpha c_\alpha^2 v_d - (\mu - \\
&\quad 2\lambda_a v_t) c_\alpha^3 + 2s_\alpha^2 c_\alpha (\mu - 2(\lambda_a - 3\lambda_b) v_t)) \\
t_4 &= iA_0(m_{H_0}^2), \\
T_4 &= iA_0(m_{h_0}^2), \\
s_4 &= \frac{1}{2},
\end{aligned} \tag{5.10}$$

$$\begin{aligned}
c_5 &\equiv c_{H_+ H_-} = -\frac{i}{2}((-2\mu c_{\theta_\pm} s_{\theta_\pm} + 2\lambda_a c_{\theta_\pm}^2 v_d + \lambda s_{\theta_\pm}^2 v_d) c_\alpha \\
&\quad + (4\lambda_b c_{\theta_\pm}^2 v_t + (\mu + 2\lambda_a v_t) s_{\theta_\pm}^2) s_\alpha) \\
C_5 &\equiv C_{H_+ H_-} = -\frac{i}{2}(2\mu c_{\theta_\pm} s_{\theta_\pm} s_\alpha + (\mu c_\alpha - \lambda v_d s_\alpha + \\
&\quad 2\lambda_a v_t c_\alpha) s_{\theta_\pm}^2 + 2(-\lambda_a v_d s_\alpha + 2\lambda_b v_t c_\alpha) c_{\theta_\pm}^2) \\
t_5 &= T_5 = 2 \times iA_0(m_{H_\pm}^2), \\
s_5 &= \frac{1}{2},
\end{aligned} \tag{5.11}$$

$$\begin{aligned}
c_6 &\equiv c_{ZZ} = iem_W c_\alpha c_{\theta_\pm} / (c_w^2 s_w), \\
C_6 &\equiv C_{ZZ} = -iem_W c_{\theta_\pm} s_\alpha / (c_w^2 s_w), \\
t_6 &= T_6 = -i((n-1)A_0(m_Z^2) + \xi_Z A_0(\xi_Z m_Z^2)), \\
s_6 &= \frac{1}{2},
\end{aligned} \tag{5.12}$$

$$\begin{aligned}
c_7 &\equiv c_{W_+ W_-} = iem_W (c_\alpha c_{\theta_\pm} - 2s_\alpha s_{\theta_\pm}) / s_w, \\
C_7 &\equiv C_{W_+ W_-} = -iem_W (c_{\theta_\pm} s_\alpha - 2c_\alpha s_{\theta_\pm}) / s_w, \\
t_7 &= T_7 = 2 \times (-i((n-1)A_0(m_W^2) + \xi_W A_0(\xi_W m_W^2))), \\
s_7 &= \frac{1}{2},
\end{aligned} \tag{5.13}$$

$$\begin{aligned}
c_8 &\equiv c_{f\bar{f}} = \frac{-i}{2}e(c_\alpha/c_{\theta_\pm})m_f/(m_W s_w), \\
C_8 &\equiv C_{f\bar{f}} = \frac{i}{2}e(s_\alpha/c_{\theta_\pm})m_f/m_W s_w, \\
t_8 &= T_8 = im_f A_0(m_f^2)Tr(I_n), \\
s_8 &= 1,
\end{aligned} \tag{5.14}$$

$$\begin{aligned}
c_9 &\equiv c_{\eta_Z \bar{\eta}_Z} = \frac{-i}{2}em_W(c_\alpha c_{\theta_\pm})\xi_Z/(c_w^2 s_w), \\
C_9 &\equiv C_{\eta_Z \bar{\eta}_Z} = \frac{i}{2}em_W(c_{\theta_\pm} s_\alpha)\xi_Z/(c_w^2 s_w), \\
t_9 &= T_9 = iA_0(\xi_Z m_Z^2), \\
s_9 &= 1,
\end{aligned} \tag{5.15}$$

$$\begin{aligned}
c_{10} &\equiv c_{\eta_\pm \bar{\eta}_\pm} = \frac{-i}{2}em_W(c_\alpha c_{\theta_\pm} - 2s_\alpha s_{\theta_\pm})\xi_W/s_w, \\
C_{10} &\equiv C_{\eta_\pm \bar{\eta}_\pm} = \frac{i}{2}em_W(c_{\theta_\pm} s_\alpha - 2c_\alpha s_{\theta_\pm})\xi_W/s_w, \\
t_{10} &= T_{10} = 2 \times iA_0(\xi_W m_W^2), \\
s_{10} &= 1,
\end{aligned} \tag{5.16}$$

Appendix C : Higgs signal strengths

Here we collect the Higgs signal strength measurements corresponding to various Higgs boson production modes and Higgs decay channels.

For the $\tau^-\tau^+$ and W^+W^- channels, we used the combined results at LHC Run 1 [42–44], whereas the Higgs to diphoton signal strength at 13 TeV [45] was considered to control the variation of the previously defined observable $R_{\gamma\gamma}$.

References

- [1] G. Aad et al. [ATLAS Collaboration], Phys. Lett. **B 716** (2012) 1.
- [2] S. Chatrchyan et al. [CMS Collaboration], Phys. Lett. **B 716** (2012) 30.

Decay channel	Production Mode	ATLAS	CMS
$\gamma\gamma$	ggF	$0.62^{+0.30}_{-0.29}$ [37]	$0.77^{+0.25}_{-0.23}$ [38]
	VBF	$2.25^{+0.75}_{-0.75}$ [37]	$1.61^{+0.90}_{-0.80}$ [38]
ZZ	ggF	$1.34^{+0.39}_{-0.33}$ [37]	$0.96^{+0.40}_{-0.33}$ [39]
	VBF	$3.8^{+2.8}_{-2.2}$ [37]	$0.67^{+1.61}_{-0.67}$ [39]
$b\bar{b}$	ggF	—	—
	VBF	$-3.9^{+2.8}_{-2.9}$ [40]	$-3.7^{+2.4}_{-2.5}$ [41]

Table 2: The Higgs signal strengths in various production and decay channels measured by ATLAS and CMS at LHC Run 2 ($\sqrt{s} = 13$ TeV).

- [3] M. Aaboud et al. [ATLAS Collaboration], Phys. Rev. D **97** (2018) 072003.
- [4] S. Chatrchyan et al. [CMS Collaboration], HIG-16-040 arXiv:1804.02716 [hep-ex]; HIG-17-012 arXiv:1804.01939 [hep-ex]; HIG-17-018 arXiv:1803.05485 [hep-ex].
- [5] M. Aoki and S. Kanemura, Phys. Rev. D **77** (2008) no.9, 095009; Erratum: [Phys. Rev. D **89** (2014) no.5, 059902].
- [6] A. G. Akeroyd and C. W. Chiang, Phys. Rev. D **81** (2010) 115007.
- [7] A. Arhrib, R. Benbrik, M. Chabab, G. Moulhaka, M. C. Peyranère, L. Rahili, and J. Ramadan, Phys. Rev. D **84** (2011) 095005.
- [8] M. Chabab, M. C. Peyranère and L. Rahili, Phys. Rev. D **90** (2014) 035026.
- [9] M. Chabab, M. C. Peyranère and L. Rahili, Phys. Rev. D **93** (2016) 115021.
- [10] P. Chardonnet, P. Salati and P. Faye, Nuc. Phys. B **394** (1993) 35.

- [11] P. F. Perez, H. H. Patel, M. J. Ramsey-Musolf and K. Wang, Phys. Rev. D **79** (2009) 055024.
- [12] S. Bahrami and M. Frank, Phys. Rev. D **91** (2015) 075003; R. N. Mohapatra and G. Senjanovic, Phys. Rev. D **23** (1981) 165; M. Magg and C. Wetterich, Phys. Lett. B **94** (1980) 61; T. P. Cheng and L.-F. Li, Phys. Rev. D **22** (1980) 2860; J. Schechter and J. W. F. Valle, Phys. Rev. D **22** (1980) 2227.
- [13] L. Wang and X. F. Han, JHEP **1403**, 010 (2014).
- [14] F. Bazzocchi and M. Fabbrichesi, Phys. Rev. D **87**, no. 3 (2013) 036001; A. Drozd, B. Grzadkowski and J. Wudka, JHEP **1204** (2012) 006; B. Grzadkowski and J. Wudka, Phys. Rev. Lett. **103** (2009) 091802.
- [15] I. Masina and M. Quiros, Phys. Rev. D **88** (2013) 093003.
- [16] I. Chakraborty and A. Kundu, Phys. Rev. D **87** (2013) 055015.
- [17] A. Biswas, and A. Lahiri, Phys. Rev. D **91** (2015) 115012.
- [18] P. Bechtle, S. Heinemeyer, O. Stal, T. Stefaniak, and G. Weiglein Eur. Phys. J C **75** (2015) 421.
- [19] C. Patrignani et al., Particle Data Group, Chin. Phys. C **40** (2016) 100001.
- [20] M. Baak et al., Gfitter Group Collaboration. Eur. Phys. J C **74** (2014) 3046.
- [21] N. Khan. Eur. Phys. J C **78** (2018) 341.
- [22] M. J. G. Veltman, Acta. Phys. Pol B **12** (1981) 437.
- [23] K. Chetyrkin and A. Kwiatkowski, Nucl. Phys. B **461** (1996) 3; A. Djouadi, J. Kalinowski and P. M. Zerwas, Z. Phys. C **70** (1996) 435.
- [24] Measurement of fiducial, differential and production cross sections in the $H \rightarrow \gamma\gamma$ decay channel with 13.3 fb^{-1} of 13 TeV proton-proton collision data with the ATLAS detector. ATLAS-CONF-2016-067.

- [25] Measurements of Higgs boson properties in the diphoton decay channel with 36.1 fb^{-1} pp collision data at the center-of-mass energy of 13 TeV with the ATLAS detector. Technical Report ATLAS-CONF-2017-045, CERN, Geneva, July 2017.
- [26] Combined measurements of Higgs boson production and decay in the $H \rightarrow ZZ^*4\ell$ and $H \rightarrow \gamma\gamma$ channels using $\sqrt{s} = 13 \text{ TeV}$ pp collision data collected with the ATLAS experiment. Technical Report ATLAS-CONF-2017-047, CERN, Geneva, July 2017.
- [27] Measurements of properties of the Higgs boson decaying into four leptons in pp collisions at $\sqrt{s} = 13 \text{ TeV}$. Technical Report CMS-PAS-HIG-16-041, CERN, Geneva, 2017.
- [28] A. Arhrib, R. Benbrik, M. Chabab, G. Moulhaka and L. Rahili, JHEP **1204** (2012) 136.
- [29] A. Arhrib, R. Benbrik, G. Moulhaka, L. Rahili, arXiv:1411.5645 [hep-ph]
- [30] A. Arhrib, Y. L. S. Tsai, Q. Yuan and T. C. Yuan, JCAP **1406** (2014) 030; N. Khan and S. Rakshit, Phys. Rev. **D 92** (2015) 055006; A. Goudelis, B. Herrmann and O. Stål, JHEP **1309** (2013) 106.
- [31] G. Abbiendi et al. [OPAL Collaboration], Eur. Phys. J. **C18** (2001) 425
- [32] J. Abdallah et al. [DELPHI Collaboration], Eur. Phys. J. **C38** (2004) 1.
- [33] J. F. Gunion, Y. Jiang, and S. Kraml, Phys. Rev. Lett. **110** (2013) 051801.
- [34] P. M. Ferreira, R. Santos, H. E. Haber and J. P. Silva, Phys. Rev. D **87** (2013) 055009.
- [35] A. Drozd, B. Grzadkowski, J. F. Gunion, and Y. Jiang, JHEP **05** (2013) 072.
- [36] J. Horejsi and M. Kladiva, Eur. Phys. J. **C 46** (2006) 81.
- [37] **ATLAS** Collaboration, “Combined measurements of the Higgs boson production and decay rates in $H \rightarrow ZZ^* \rightarrow 4\ell$ and $H \rightarrow \gamma\gamma$ final states using pp collision data at $\sqrt{s} = 13 \text{ TeV}$ in the ATLAS experiment,” Tech. Rep. ATLAS-CONF-2016-081, CERN, Geneva, Aug, 2016. <http://cds.cern.ch/record/2206272>.

- [38] **CMS** Collaboration, “Updated measurements of Higgs boson production in the diphoton decay channel at $\sqrt{s} = 13$ TeV in pp collisions at CMS,” Tech. Rep. CMS-PAS-HIG-16-020, CERN, Geneva, 2016. <https://cds.cern.ch/record/2205275>.
- [39] **CMS** Collaboration, “Measurements of properties of the Higgs boson and search for an additional resonance in the four-lepton final state at $\sqrt{s} = 13$ TeV,” Tech. Rep. CMS-PAS-HIG-16-033, CERN, Geneva, 2016. <https://cds.cern.ch/record/2204926>.
- [40] **ATLAS** Collaboration, “Search for Higgs boson production via weak boson fusion and decaying to $b\bar{b}$ in association with a high-energy photon in the ATLAS detector,” Tech. Rep. ATLAS-CONF-2016-063, CERN, Geneva, Aug, 2016. <http://cds.cern.ch/record/2206201>.
- [41] **CMS** Collaboration, “Search for the standard model Higgs boson produced through vector boson fusion and decaying to bb with proton-proton collisions at $\sqrt{s} = 13$ TeV,” Tech. Rep. CMS-PAS-HIG-16-003, CERN, Geneva, 2016. <https://cds.cern.ch/record/2160154>.
- [42] G. Aad et al. [ATLAS Collaboration], Phys. Rev. **D 92** (2015) 012006.
- [43] S. Chatrchyan et al. [CMS Collaboration], JHEP **01** (2014) 096;
- [44] G. Aad et al. [ATLAS Collaboration], “Evidence for Higgs boson Yukawa couplings in the $H \rightarrow \tau\tau$ decay mode with the ATLAS detector,” Tech. Rep. ATLAS-CONF-2014-061, CERN, Geneva, Oct, 2014.
- [45] G. Aad et al. [ATLAS Collaboration], “Measurement of fiducial, differential and production cross sections in the $H \rightarrow \gamma\gamma$ decay channel with 13.3 fb^{-1} of 13 TeV proton-proton collision data with the ATLAS detector”, ATLAS-CONF-2016-067 (2016).